HHS Public Access

Author manuscript

ACS Nano. Author manuscript; available in PMC 2017 December 27.

Published in final edited form as:

ACS Nano. 2016 December 27; 10(12): 11127–11135. doi:10.1021/acsnano.6b05995.

Kinetics of T3-DNA Ligase-Catalyzed Phosphodiester Bond Formation Measured using the α-Hemolysin Nanopore

Cherie S. Tan, **Jan Riedl**, **Aaron M. Fleming**, **Cynthia J. Burrows***, and **Henry S. White***

Department of Chemistry, University of Utah, 315 South 1400 East, Salt Lake City, Utah 84112-0850, United States

Abstract

The latch region of the wild-type α-hemolysin (α-HL) protein channel can be used to distinguish single base modifications in double-stranded DNA (dsDNA) *via* ion channel measurements upon electrophoretic capture of dsDNA in the vestibule of α-HL. Herein, we investigated the use of the latch region to detect a nick in the phosphodiester DNA backbone. The presence of a nick in the phosphodiester backbone of one strand of the duplex results in a significant increase in both the blockade current and noise level relative to the intact duplex. Differentiation between the nicked and intact duplexes based on blockade current or noise, with near baseline resolution, allows real-time monitoring of the rate of T3-DNA ligase-catalyzed phosphodiester bond formation. Under low ionic strength conditions containing divalent cations and a molecular crowding agent (75 mg ml^{-1} PEG), the rate of enzyme-catalyzed reaction in the bulk solution was continuously monitored by electrophoretically capturing reaction substrate or product dsDNA in the α-HL protein channel vestibule. Enzyme kinetic results obtained from the nanopore experiments match those from gel electrophoresis under the same reaction conditions, indicating the α-HL nanopore measurement provides a viable approach for monitoring enzymatic DNA repair activity.

Graphical Abstract

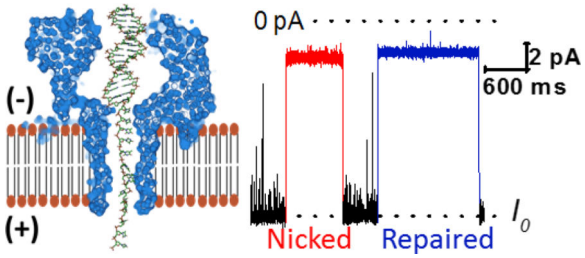

Keywords

α-hemolysin; latch zone; nicked duplex; DNA ligase; enzyme kinetics

Correspondence: burrows@chem.utah.edu and white@chem.utah.edu.

Conflict of Interest: The authors declare no competing financial interest.

Supporting Information. The Supporting Information is available free of charge on the ACS Publications website at DOI:xxx. Melting temperatures measurement, current-time traces, current blocking histograms, current noise histograms, repeated ligase process measurements, and calculation of standard error of the mean.

INTRODUCTION

We report the use of the α-hemolysin (α-HL) latch zone, a 2.6 nm vestibule constriction zone (Figure 1a), to measure the rate of phosphodiester bond formation catalyzed by T3-DNA ligase. Phosphodiester backbone breaks are produced directly by damaging agents (ionizing radiation or ultraviolet light),[1–2] or as intermediates during DNA replication and recombination, as well as during DNA repair, such as base excision, nucleotide excision, and mismatch repair).[2–5] In the cell, DNA strand breaks can be repaired by a multi-protein pathway that involves a DNA ligase in the last step to create a phosphodiester bond.[2–5] However, unrepaired DNA strand breaks from abortive DNA ligation events are lethal, especially in neuronal cells.[6–8] There is a fundamental gap in understanding the kinetic steps of ligation, in part, due to the lack of a fast *in vitro* method for monitoring nick repair.[7–8] Herein, we demonstrate that a single nick in an individual dsDNA molecule can be identified from an intact duplex in ion channel recordings using α-HL, allowing kinetic analysis of the ligation reaction. These studies add to the growing body of literature using biological nanopore as a tool to investigate enzyme activity.[9]

Analysis of duplex DNA is achieved by electrophoretically driving dsDNA with a single-stranded tail into the vestibule of the α-HL protein channel as depicted in Figure 1a.[10–13] A single duplex is captured in the vestibule by threading the single-stranded tail through the narrow β-barrel.[11–13] The duplex occupies the vestibule of α-HL because its diameter (2.0 nm) is larger than the 1.4 nm central constriction of α-HL (Figure 1a), preventing entry of the duplex into the β-barrel.[10–15] Ion current flowing through the nanopore is blocked by the trapped DNA resulting in a reduction in current prior to unzipping of the duplex into its single-strand components.[15–17] Correlations between the blockade current and unzipping time with the DNA duplex structure have been made; for example, unzipping time generally increases with the thermal stability of the duplex, while sequence context influences the blocking current level.[12–13, 18–19] We previously utilized the difference in current level associated with a single base modification in dsDNA to measure uracil-DNA glycosylase (UDG) activity, by monitoring the rate of conversion of a uracil to an abasic site.[20] Further investigation of the latch constriction of α-HL has demonstrated that one G:C base pair can be distinguished from an A:T pair, as well as single-base mismatches (e.g., C:C or C:A), based on current blockade levels.[21–22] Recently, we also observed that mismatched base pairs induce characteristic ion current modulations in the α-HL channel.[22–23]

In this article, we demonstrate that the latch region can be used to differentiate duplexes with and without a break in the phosphate backbone, not only by the difference in blockade currents but also by the difference in the current noise level. The formation of a phosphodiester bond by a ligase was continuously monitored in real-time without radioactive or fluorescent labels allowing determination of the enzyme-catalyzed rate constant. Our results extend the application of the α-HL protein channel as a general *in vitro* tool to investigate the kinetics of enzymes operating on DNA.

RESULTS AND DISCUSSION

A 41-mer target strand comprising a 24-mer poly-dT tail at the 5' end and a 17-mer heterosequence, 5'-$(T)_{24}$-TGGAGCTGGTGGCGTAG, was used throughout this study. This sequence encompasses codon 12 of the *KRAS* gene for which frequent mutations have been observed resulting from DNA base damage in cancer samples.[24–25] Incomplete repair of the DNA base damage would lead to a nick in this sequence context. In this study, we compare the *I-t* characteristics of a duplex containing a nick, synthesized by hybridizing the 41-mer target to a complementary 9-mer (5'-CTACGCCAC) and a modified 8 mer with a 5'-phosphate (5'-pCAGCTCCA), to that of a 41-mer target bound to a complementary 17-mer probe, the latter representing a standard for the intact DNA duplex (Figure 1). In previous work, we demonstrated that the blunt end of the duplex is not captured in the α-HL vestibule at low salt concentration (< 150 mM).[20] In contrast, when the poly$(T)_{24}$ tail is treaded into the β-barrel, the nick is located in proximity of the latch region as shown in Figure 1a.[20, 26] The current-time trace (*I-t*) of each captured event provides a unique electrical signature allowing identification of either the nicked or repaired duplex.

DNA ligases are magnesium-dependent DNA repair enzymes that utilize either ATP or NAD^+ to catalyze the formation of the phosphodiester bond between adjacent 5'-phosphate and 3'-hydroxyl termini of nick-containing dsDNA.[27–28] The ATP-dependent ligases possess a common core structure that is observed in the T series ligases found in bacteriophages.[29–31] In this report, we aim to demonstrate that the α-HL nanopore is a general enzymology tool to obtain kinetic information for ligases. Low salt (~180 mM electrolyte) conditions were employed: 100 mM KCl, 66 mM Tris·HCl, 5 mM $MgCl_2$, 1 mM ATP, 7.5% (w/v) polyethylene glycol 6000 (PEG 6000), pH 7.6 at 20.0 °C.

In general, monovalent cations disturb the electrostatic interactions between ligases and DNA strands, and therefore most DNA ligases work favorably under low salt conditions with less than 100 mM monovalent cations.[32–36] However, the α-HL nanopore analysis is based on ion channel electrical measurements and requires significant electrolyte concentration to detect changes in the electrical current.[32, 37] In order to minimize the influence of monovalent cations, which perturb the activity of DNA ligase, polyethylene glycol (PEG) was added to the electrolyte to enhance the hydrophobic interactions between the ligase and DNA strands.[38–39] PEG 6000 was added to the electrolyte at 75 mg/mL, acting as a volume excluder to increase the local concentration of the DNA and to enhance the activity of the enzyme.[38–41] However, PEG and potassium ions form a positively charged complex (PEG-K^+), which by itself is reported to interact with α-HL.[42] While PEG 6000 is too large to be completely accommodated in the channel, it can potentially partially enter and then withdraw from the vestibule, generating an interfering blockade current.[42–46] Thus, in order to prevent PEG-K^+ complex capture, PEG was added only in the *cis* side of the channel, where it is electrically driven away from the α-HL nanopore and, thus, it does not contribute to the current signature under the applied negative bias (*cis* vs. *trans*). Control experiments indicated that none of the buffer components (7.5% PEG (w/v) as volume excluder, 1 mM ATP and 5 mM $MgCl_2$) interact with α-HL to produce measureable electrical signals (Figure S1).

We performed experiments to determent if the latch region of α-HL could be used to identify the presence of a single-strand break in the DNA backbone, as schematically depicted in Figure 1. In a typical experiment, duplex DNA at a concentration of 14 μM, was added to the 350-μL *cis* reservoir, and a bias of −120 mV (*cis* vs. *trans*) was applied to electrophoretically capture individual duplexes. For each duplex, a 5-fold excess of the short probe strands (8-, 9- or 17-mer) versus target strands (41-mer) was added to the solution; the two resulting types of events, corresponding to either excess ssDNA translocation or dsDNA unzipping, are readily differentiated by the order of magnitude difference in the event duration time, *t*, as will be discussed below.

The nicked duplex corresponds to the 41-mer target bound simultaneously to *both* the 8- and 9-mer complementary probes. However, when these three ssDNA strands (41-, 8-, and 9-mer) are in the same solution, there are three distinct duplexes due to the duplex-ssDNA equilibria. In addition to the nicked dsDNA, there are two possible duplexes where only one probe is bound to the 41-mer target, either 41:8 dsDNA or 41:9 dsDNA. Thus, an excess amount of 8-mer or 9-mer is needed to favor nicked duplex formation.

We first studied the 41-mer strand bound separately to each of the 8- or 9-mer probes (Figure 2a–b and S2). At −120 mV (*cis* vs. *trans*), the addition of 41:8 or 41:9 duplex with 5-fold excess of 8- or 9-mer probes in the *cis* reservoir generated frequent and characteristic current blockades. The excess 8- or 9-mer probes generated fast current blockade events (< 0.5 ms) with broad current distributions (Figure 2c), which are caused by either ssDNA translocation or short transient collisions between DNA strands and the protein channel, as previously reported.[47] Because excess ssDNA probe strands (8 or 9-mer) do not fully occupy the β-barrel during translocation, the ssDNA probe events do not generate full blockades that can be readily distinguished from the collision events. Conversely, the translocation events for the 41-mer (circled in white) are clearly separated from the collision events, and the event population density is centered at −2.9 pA blocking current with 0.45 ms dwell time (Figure 2c and S3).

Interestingly, the unzipping event signatures of the two 41:8 and 41:9 duplexes are very different. Blockade events in a solution containing the 41:9 duplex clearly fall into two populations, comprising short current spikes for excess 9-mer ssDNA translocation, and relatively long current blockade events (1–100 ms) corresponding to 41:9 duplex unzipping. On the other hand, 41-mer ssDNA translocation events were observed in solution containing the 41:8 duplex, in addition to the expected excess 8-mer ssDNA translocation and 41:8 duplex unzipping event, as shown in the scatter plot (circled in white, Figures 2c and S2). This observation indicates that the fraction of 41-mer hybridized with 8-mer (~50%) was significantly smaller compared to 41-mer with 9-mer probe (~95%), consistent with the stability of the 41:9 duplex being greater than that of the 41:8 duplex (Figure S4).

The longer blockade events (1–100 ms) of the 41:8 or 41:9 duplex reflect the time for the duplex to unzip into two ssDNA strands. There is a single unzipping population in the blockade current histogram for 41:9 duplex (the peak at −4.1 pA, Figure 3a–b), however, the blockade current distribution of 41:8 duplex unzipping events displays a primary peak at –4.1 pA and a minor peak at −3.4 pA (Figure 3a–b). These distributions of the blockade

currents for the 41:8 duplex (Figure 3b) correspond to either 5’ or 3’ tail entry into the protein channel. As has been reported, 3’ entry of ssDNA generates a deeper blockade than 5’ entry;[13, 48–51] therefore, the primary peak at −4.1 pA is assigned as 5’-homo$(dT)_{24}$ entry and the minor peak at −3.4 pA corresponds to the 3’-hetero$(dN)_9$ entry. Even though 3’ entry is generally reported as being favored,[13, 51] the length of the overhang dominates the duplex capture rate,[52] resulting in a favorable entry direction of 5’-homo$(dT)_{24}$ overhang in comparison to the 3’-hetero$(dN)_9$ tail.

The unzipping duration time corresponds to the duplex stability, which was also examined for the 41:8 and 41:9 duplexes. The temporal dispersion of the unzipping events for each duplex is approximated by an exponential decay with a time decay constant, τ, equal to 1.8 ± 0.1 ms and 11.0 ± 0.6 ms, for the 41:8 and 41:9 duplexes, respectively (Figure 3c). This 6-fold difference in τ might be due to the difference in stability as mentioned above, or due to the greater latch zone restriction on the 41:9 duplex compared with 41:8 duplex, as will be discussed below. Overall, the 41:8 duplex is considerably less stable relative to the 41:9 duplex. In order to promote the annealing of the 8-mer probe to the 41-mer target, and also increase the proportion of nicked DNA in the solution compared to the 41:8 and 41:9 duplexes, a 5-fold excess of the 8-mer probe strand was employed to study the nicked DNA (1:5:1 amount ratio of 41 mer: 8 mer: 9 mer).

The ability of α-HL to discriminate between nicked dsDNA with a single backbone break and the repaired duplex was examined by performing nanopore unzipping experiments. With either nicked or repaired duplexes at a concentration of 14 μM, we observed that the two duplexes generated unique current signatures while residing in the protein channel prior to unzipping, with the nicked duplex blockade current magnitude being ~0.5 pA higher than the repaired one (Figure 4). The blockade current histograms for individual nicked (−3.5 pA) and repaired duplexes (−3.0 pA) display very narrow distributions with 0.1 pA FWHM (full width at half maximum), Figure 4a–b. Experiments in which both duplexes were present in solution demonstrate nearly baseline resolved blockade current histograms, again with 0.1 pA FWHM for each peak (Figure 4d). Equal capture rates are observed for the two duplexes, as indicated by the similar areas of the two histograms. Unlike previous α-HL analyses of single base modification to duplexes,[20–22, 26, 51, 53] the only difference between the nicked duplex and repaired duplex is the presence of a single P-O bond, as shown in Figure 1b and c. The observed ~0.5 pA current difference between the nicked and repaired duplexes is likely due to one additional negative charge, the PO_4^{2-} on the 5’ end of the 8-mer probe, which we speculate may increase the local counter-ion concentration at the latch zone in addition to modulating the ion flux blockade *via* duplex structure modification, as previously reported for single base recognition.[13, 21, 51]

It is known that the unzipping time duration of a DNA duplex is correlated with the duplex thermal stability, as well as the G•C content adjacent to the overhang.[19, 51] A 25 °C increase in the melting temperature between the nicked and repaired duplexes with the same sequence but differing by a single phosphodiester bond break is observed (Figure S4). However, the two duplexes were not themselves distinguishable by their unzipping duration times. As shown in Figure 5, the histograms of duration time for the nicked and repaired DNA displayed first-order exponential kinetics with time constants of 840 ± 60 ms and 950

± 40 ms, respectively. The stability of each duplex was measured by melting temperature measurements in the bulk solution, where both the 5' and 3' termini of either 8- or 9-mer could detach from the 41-mer target. T_m = 46 ± 1 °C for the nicked duplex while T_m = 71 ± 1 °C for intact duplex (Figure S4). These T_m values would suggest much faster unzipping for the nicked duplex, in contrast to the experimental observation. However, when the nicked duplex was captured by the protein channel, the 2.6 nm latch zone restricts the mobility of the adjacent 5'-phosphate and 3'-hydroxyl termini. This confinement appears to increase the stability of the nicked duplex, resulting in a longer exponential decay time constant than would be predicted from the T_m value.[51]

Evidence for the interaction between the nicked duplex and the latch zone is also inferred from the noise of each individual blockade current event. As shown in Figure 6, the nicked and repaired duplexes can be distinguished by either noise or blockade current. The noise for the nicked duplex unzipping events displayed a distribution centered at 0.45 pA, while that for the intact DNA is centered at a 0.35 pA. As over 99.5% of the nicked DNA unzipping events exhibit noise greater than 0.40 pA (Figure 6a), the events with noise less than 0.40 pA can be assigned to repaired duplexes. Figure 6d shows the population density plot for blockade noise as a function of blockade current for a solution containing both nicked and repaired duplexes, demonstrating that the two duplexes can be clearly distinguished based on their *I-t* signatures.

In a previously reported study, the unzipping event noise level normalized to the open-channel noise (the median of the event noise divided by the median of the open-channel noise) was correlated to the duplex stability.[26] In general, a duplex with a 5 °C increase in T_m value results in ~ 0.3 decrease in normalized noise.[26] However, in this study the normalized noise for nicked (0.61) and repaired (0.48) DNA were only 0.13 different despite a 25 °C difference in the T_m value (T_m = 46 ± 1 °C for nicked DNA and T_m = 71 ± 1 °C for repaired DNA), suggesting the nicked DNA is stabilized by the latch zone of the protein channel relative to the bulk solution, as mentioned earlier. On the other hand, the near-baseline resolved separation of the two duplexes, and a broader distribution of the current noise of the nicked duplex compared to the repaired one, indicates that the interactions between the latch zone and the two types of duplex are very different. The higher noise associated with the nicked DNA is probably due to the dynamics of the 3'-OH and 5'-PO_4 termini in the latch zone.

The ability to identify nicked and intact duplexes based on either blockade current or noise suggests that the conversion of the nicked DNA to the repaired (intact) duplex in bulk solution by a DNA ligase can be monitored by counting single-molecule unzipping events in the α-HL protein channel (Figure 7). Nicked dsDNA (14 μM) was added to the 350-μL *cis* reservoir, containing 100 mM KCl, 66 mM Tris-HCl, 7.5% PEG (w/v), 1 mM ATP and 5 mM $MgCl_2$. Events displaying a single blockade current were observed (Figure 7b top left histogram), corresponding to the nicked duplex. After addition of T3-DNA ligase (540 nM), events with a smaller blockade current corresponding to the repaired duplex appeared in the *I-t* trace, indicating enzyme-catalyzed phosphodiester bond formation. The identity of the repaired duplex was confirmed from the current amplitude and current noise of the unzipping events, with −3.45 ± 0.03 pA (noise ≥ 0.40 pA) being attributed to the starting

material and −3.04 ± 0.03 pA (noise < 0.40 pA) to the product, consistent with the results of the control experiments shown in Figures 4 and 6. The ligase-catalyzed phosphodiester bond formation was monitored through the time-dependent histograms of blockade currents (Figure 7b) and noise histograms (Figure S8), in which the relative peak areas (counts) for the two species were used to monitor the enzyme kinetics, as shown in Figure 8.

The percentage of the repaired duplex as a function of reaction time obtained from nanopore experiments is plotted in Figure 8 and compared with values obtained from gel electrophoresis under identical reaction conditions. The reaction time plotted in Figure 8 corresponds to the midpoint of the time window used to obtain each histogram. The reaction rate of T3-DNA ligase in the nanopore experiment obtained from the linear slope (Figure 8 blue circle at 2.5 min time point) is 0.8 ± 0.2 nmol/min, which is in a good agreement with the value from gel electrophoresis (Figure 8 green triangle at the 5 min time point), 0.7 ± 0.1 nmol/min. In separate experiments, the same concentration of nicked DNA substrate (14 μM) was catalyzed by 360 and 450 nM T3-DNA ligase, and product formation was measured by blockade currents as shown in Figure 8. We find that the reaction rates (the linear slopes in Figure 8) are proportional to the ligase concentration and independent of substrate concentration. Therefore, these enzyme kinetic curves demonstrate that the ligase-catalyzed phosphodiester bond formation reaction is zero order initially and then slows as the reaction reaches completion. However, with 360 nM T3-DNA ligase the percentage product conversion is 53% conversion after 5 hours (Figure S10), which is probably due to the deactivation of the enzyme over a period of time.

As discussed earlier, high cation concentrations inhibit ligase activity; for instance, virtually no ligated product was generated with more than 200 mM KCl for the T4 DNA ligase,[33] and 100 mM NaCl completely inhibited *Methanocaldococcus jannaschii* DNA ligase.[35] Interestingly, T3 DNA ligase activity is T3 DNA ligase activity is reported to increase up to 300 mM and remains relatively constant up to 1 M.[31] We investigated T3 DNA ligase activity is solutions containing 100, 300, and 1000 mM KCl in the presence of 66 mM Tris-HCl and 5 mM $MgCl_2$. We observe that the repaired duplex is not detected by either the nanopore system or by gel electrophoresis at 1M KCl, as shown in Figure S12, and that maximum enzymatic activity is achieved at 100 mM KCl (Figure S9, S12). Nanopore measurements at lower KCl concentrations are prohibited by the electrical noise limit.

CONCLUSIONS

The work presented here demonstrates that the latch zone of α-HL can be utilized to monitor the kinetics of ligase-catalyzed phosphodiester bond formation under complex electrolyte conditions. These results and our previous report of monitoring the UDG-catalyzed conversion of a uracil to an abasic site indicate the general utility of the α-HL protein nanopore as a DNA enzymology tool. We have now demonstrated that DNA backbone lesions can be identified by current noise analysis in addition to the normal blockade current differentiation, suggesting the potential development of new methods to differentiate various DNA lesions. Use of the α-HL protein to investigate complex multistep enzyme kinetics, such as in the base-excision repair pathway, is now a possible goal.

EXPERIMENTAL SECTION

DNA Preparation and Purification

All ssDNA strands were synthesized from commercially available phosphoramidites (Glen Research, Sterling, VA) and prepared by the DNA/peptide core facility at the University of Utah. The DNA purification process was achieved by HPLC using an anion-exchange column running a linear gradient of B from 1% to 100% over 30 min (A = 10% CH_3CN/90% ddH_2O, B = 20 mM NaP_i, 1 M NaCl, pH 7, in 10% CH_3CN/90% ddH_2O, flow rate = 3 mL/min) while monitoring the DNA strand elution by the UV absorbance at 260 nm. The purification salts were removed by dialysis against ddH_2O for 36 h at 4 °C. The dialyzed samples were dried by lyophilization and then resuspended in ddH_2O. The concentrations of the DNA solutions were obtained by measuring the absorbance at 260 nm and using the primary sequence to estimate the extinction coefficient.

Glass Nanopore Membrane (GNM) and Bilayer Formation for Ion Channel Recording

A conical shaped nanopore was fabricated in a sealed capillary using a bench-top method.[54] Nanopores with a 500 to 1000 nm radius were used for the experiments. The GNM surface was silanized by 2% (3-cyanopropyl)dimethylchlorosilane in acetonitrile to make the glass surface hydrophobic allowing the formation of a lipid bilayer across the orifice.

Chemicals and Materials for Nanopore Measurement

The lipid bilayer was formed by 1,2-diphytanoyl-*sn*-glycero-3-phospho-choline (DPhPC) dissolved in decane at 10 mg/mL. The wild-type α-HL monomer was purchased from List Biological Laboratories as a lyophilized powder and dissolved in water at 0.2 mg/mL. Buffer A (100 mM KCl, 66 mM Tris·HCl, 7.5% PEG, 5 mM $MgCl_2$, 1 mM ATP, at pH 7.6) was placed outside the capillary, which was the *cis* site of α-HL. Buffer B (100 mM KCl 66 mM Tris-HCl at pH 7.6) was used to fill the capillary to avoid the PEG molecule blocking the outlet of the DNA molecules. T3-DNA ligase at 3×10^6 units/mL and its cofactor ATP were purchased from New England Biolabs, Ipswich, MA. The volume excluder polyethylene glycol 6000 (PEG 6000) was purchase from Sigma.

Gel electrophoresis analysis

The same reaction conditions with buffer B were used to conduct the T3-DNA ligase activity measurements. 5 nmol (14 μM) of 41-mer template strand was hybridized with the same amount of 9-mer probe, and a 5-fold molar excess of 8 mer probe (1:5:1 amount ratio of 41 mer: 8 mer: 9 mer). The reaction was treated with 200 μmol (540 nM) of T3-DNA ligase in the 350-μL solution reservoir at 20.0 °C in the 100 mM KCl, 66 mM Tris·HCl, 7.5% PEG, 5 mM $MgCl_2$ and 1 mM ATP solution.

The analysis was conducted with a 9-mer strand that contained a FAM fluorophore at the 5′-end. Upon commencement of the reaction with the addition of T3-DNA ligase, 5-μL aliquots were removed at 5, 10, 15, 20, 30, 40, 60, 90 min time points. The reaction in each aliquot was quenched by adding 2 μL of 0.5% SDS and 50 mM EDTA and heating at 90 °C for 5 min. The ligated strands (product) were separated from the short strands (reactant) on a 20%

polyacrylamide gel that was run at 45 W for 1.5 h. Reactions were visualized and quantified by fluorescence of the FAM fluorophore on a phosphorimager.

Current−Time Recordings

Current−time (*I*−*t*) recordings were performed at 20.0 ± 0.5 °C using a custom-built high-impedance and low-noise system (Electronic BioSciences Inc., San Diego, CA). The *I*−*t* traces for duplex unzipping and ssDNA translocation events were filtered at 10 kHz (sampled at 50 kHz) and 100 kHz (sampled at 500 kHz), respectively. The voltage was applied between two Ag/AgCl electrodes, which were placed inside and outside the capillary. A pressure of 40 to 80 mmHg was applied to the inside of the GNM capillary using a gas-tight syringe to facilitate the insertion of a protein ion channel in the lipid bilayer. For α-HL insertion, 1 μL of monomer solution in water at 0.2 mg/mL was carefully added into the solution outside of the GNM. A voltage of 120 mV (*trans* vs. *cis*) was applied across the GNM to drive electrophoretically the ssDNA and dsDNA into the vestibule of the α-HL.

Data Collection

Based on a previous report, *I*-*t* blockades that lasted longer than 10 ms were identified as DNA unzipping events for 17-mer duplexes and shorter events were attributed to translocation of excess ssDNA.[13] The current amplitude and associated noise of each blockade was used to identify the duplex (nicked and repaired DNA), as described in the Results and Discussion. Events were extracted and post filtered at 5 kHz for data analysis using QuB (version 2.0.0.33). Density plots of unzipping durations were plotted using data analysis programs provided by Electronic Biosciences Inc., San Diego, CA. Histograms of current, noise, and unzipping duration were generated and plotted using Origin Pro (version 9.0). The percentage of repaired DNA (the product of the DNA ligase reaction) was obtained by counting the number of events in the product peak of the current blockade histogram and dividing it to the total number of events for both the product and the reactant in the current blockade histogram. Details of error treatment are given in the Supporting Material.

Supplementary Material

Refer to Web version on PubMed Central for supplementary material.

Acknowledgments

The authors thank Electronic Biosciences Inc. (San Diego, CA) for donating the ion-channel recording instruments and software. This work was funded by a grant from the National Institutes of Health (R01 GM093099).

REFERENCES AND NOTES

1. Cook PR, Brazell IA. Detection and Repair of Single-Strand Breaks in Nuclear DNA. Nature. 1976; 263:679–682. [PubMed: 980113]
2. Sancar A, Lindsey-Boltz LA, Unsal-Kacmaz K, Linn S. Molecular Mechanisms of Mammalian DNA Repair and the DNA Damage Checkpoints. Annu. Rev. Biochem. 2004; 73:39–85. [PubMed: 15189136]
3. Iyer RR, Pluciennik A, Burdett V, Modrich PL. DNA Mismatch Repair: Functions and Mechanisms. Chem. Rev. 2006; 106:302–323. [PubMed: 16464007]

4. Varlet I, Canard B, Brooks P, Cerovic G, Radman M. Mismatch Repair in Xenopus Egg Extracts: DNA Strand Breaks Act as Signals Rather Than Excision Points. Proc. Natl. Acad. Sci. U.S.A. 1996; 93:10156–10161. [PubMed: 8816768]
5. Morita R, Nakane S, Shimada A, Inoue M, Iino H, Wakamatsu T, Fukui K, Nakagawa N, Masui R, Kuramitsu S. Molecular Mechanisms of the Whole DNA Repair System: A Comparison of Bacterial and Eukaryotic Systems. J. Nucleic Acids. 2010; 2010:179594–179625. [PubMed: 20981145]
6. Gao Y, Sun Y, Frank KM, Dikkes P, Fujiwara Y, Seidl KJ, Sekiguchi JM, Rathbun GA, Swat W, Wang J, Bronson RT, Malynn BA, Bryans M, Zhu C, Chaudhuri J, Davidson L, Ferrini R, Stamato T, Orkin SH, Greenberg ME, et al. A Critical Role for DNA End-Joining Proteins in Both Lymphogenesis and Neurogenesis. Cell. 1998; 95:891–902. [PubMed: 9875844]
7. Ahel I, Rass U, El-Khamisy SF, Katyal S, Clements PM, McKinnon PJ, Caldecott KW, West SC. The Neurodegenerative Disease Protein Aprataxin Resolves Abortive DNA Ligation Intermediates. Nature. 2006; 443:713–716. [PubMed: 16964241]
8. Tumbale P, Williams JS, Schellenberg MJ, Kunkel TA, Williams RS. Aprataxin Resolves Adenylated Rna-DNA Junctions to Maintain Genome Integrity. Nature. 2014; 506:111–115. [PubMed: 24362567]
9. Cao C, Ying YL, Hu ZL, Liao DF, Tian H, Long YT. Discrimination of Oligonucleotides of Different Lengths with a Wild-Type Aerolysin Nanopore. Nat. Nanotechnol. 2016; 11:713–718. [PubMed: 27111839]
10. Song L, Hobaugh MR, Shustak C, Cheley S, Bayley H, Gouaux JE. Structure of Staphylococcal Alpha-Hemolysin, a Heptameric Transmembrane Pore. Science. 1996; 274:1859–1866. [PubMed: 8943190]
11. Mathe J, Visram H, Viasnoff V, Rabin Y, Meller A. Nanopore Unzipping of Individual DNA Hairpin Molecules. Biophys. J. 2004; 87:3205–3212. [PubMed: 15347593]
12. Sauer-Budge AF, Nyamwanda JA, Lubensky DK, Branton D. Unzipping Kinetics of Double-Stranded DNA in a Nanopore. Phys. Rev. Lett. 2003; 90:238101–238123. [PubMed: 12857290]
13. Jin Q, Fleming AM, Burrows CJ, White HS. Unzipping Kinetics of Duplex DNA Containing Oxidized Lesions in an Alpha-Hemolysin Nanopore. J. Am. Chem. Soc. 2012; 134:11006–11011. [PubMed: 22690806]
14. Drew HR, Wing RM, Takano T, Broka C, Tanaka S, Itakura K, Dickerson RE. Structure of a B-DNA Dodecamer: Conformation and Dynamics. Proc. Natl. Acad. Sci. U.S.A. 1981; 78:2179–2183. [PubMed: 6941276]
15. Vercoutere W, Winters-Hilt S, Olsen H, Deamer D, Haussler D, Akeson M. Rapid Discrimination among Individual DNA Hairpin Molecules at Single-Nucleotide Resolution Using an Ion Channel. Nat. Biotechnol. 2001; 19:248–252. [PubMed: 11231558]
16. Vercoutere WA, Winters-Hilt S, DeGuzman VS, Deamer D, Ridino SE, Rodgers JT, Olsen HE, Marziali A, Akeson M. Discrimination among Individual Watson-Crick Base Pairs at the Termini of Single DNA Hairpin Molecules. Nucleic Acids Res. 2003; 31:1311–1318. [PubMed: 12582251]
17. Lathrop DK, Ervin EN, Barrall GA, Keehan MG, Kawano R, Krupka MA, White HS, Hibbs AH. Monitoring the Escape of DNA from a Nanopore Using an Alternating Current Signal. J. Am. Chem. Soc. 2010; 132:1878–1885. [PubMed: 20099878]
18. Jin Q, Fleming AM, Ding Y, Burrows CJ, White HS. Structural Destabilization of DNA Duplexes Containing Single-Base Lesions Investigated by Nanopore Measurements. Biochemistry. 2013; 52:7870–7877. [PubMed: 24128275]
19. Ding Y, Fleming AM, White HS, Burrows CJ. Internal Vs Fishhook Hairpin DNA: Unzipping Locations and Mechanisms in the Alpha-Hemolysin Nanopore. J. Phys. Chem. B. 2014; 118:12873–12882. [PubMed: 25333648]
20. Jin Q, Fleming AM, Johnson RP, Ding Y, Burrows CJ, White HS. Base-Excision Repair Activity of Uracil-DNA Glycosylase Monitored Using the Latch Zone of Alpha-Hemolysin. J. Am. Chem. Soc. 2013; 135:19347–19353. [PubMed: 24295110]
21. Ding Y, Fleming AM, White HS, Burrows CJ. Differentiation of G:C Vs A:T and G:C Vs G:Mc Base Pairs in the Latch Zone of Alpha-Hemolysin. ACS Nano. 2015; 9:11325–11332. [PubMed: 26506108]

22. Johnson RP, Fleming AM, Beuth LR, Burrows CJ, White HS. Base Flipping within the Alpha-Hemolysin Latch Allows Single-Molecule Identification of Mismatches in DNA. J. Am. Chem. Soc. 2016; 138:594–603. [PubMed: 26704521]
23. Johnson RP, Perera RT, Fleming AM, Burrows CJ, White HS. Energetics of Base Flipping at a DNA Mismatch Site Confined at the Latch Constriction of A-Hemolysin. Faraday Discuss. 2016 [Online] http://dx.doi.org/10.1039/C6FD00058D.
24. Husgafvel-Pursiainen K, Hackman P, Ridanpaa M, Anttila S, Karjalainen A, Partanen T, Taikina-Aho O, Heikkila L, Vainio H. K-Ras Mutations in Human Adenocarcinoma of the Lung: Association with Smoking and Occupational Exposure to Asbestos. Int. J. Cancer. 1993; 53:250–256. [PubMed: 8425762]
25. Pfeifer GP, Besaratinia A. Mutational Spectra of Human Cancer. Hum. Genet. 2009; 125:493–506. [PubMed: 19308457]
26. Johnson RP, Fleming AM, Jin Q, Burrows CJ, White HS. Temperature and Electrolyte Optimization of the Alpha-Hemolysin Latch Sensing Zone for Detection of Base Modification in Double-Stranded DNA. Biophys. J. 2014; 107:924–931. [PubMed: 25140427]
27. Lehnman IR. DNA Ligase: Structure, Mechanism, and Function. Science. 1974; 186:790–797. [PubMed: 4377758]
28. Tomkinson AE, Vijayakumar S, Pascal JM, Ellenberger T. DNA Ligases: Structure, Reaction Mechanism, and Function. Chem. Rev. 2006; 106:687–699. [PubMed: 16464020]
29. Subramanya HS, Doherty AJ, Ashford SR, Wigley DB. Crystal Structure of an Atp-Dependent DNA Ligase from Bacteriophage T7. Cell. 1996; 85:607–615. [PubMed: 8653795]
30. Rossi R. Functional Characterization of the T4 DNA Ligase: A New Insight into the Mechanism of Action. Nucleic Acids Res. 1997; 25:2106–2113. [PubMed: 9153309]
31. Cai L, Hu C, Shen S, Wang W, Huang W. Characterization of Bacteriophage T3 DNA Ligase. J. Biochem. 2004; 135:397–403. [PubMed: 15113838]
32. Hayashi K, Nakazawa M, Ishizaki Y, Obayashi A. Influence of Monovalent Cations on the Activity of T4 DNA Ligase in the Presence of Polyethylene Glycol. Nucleic Acids Res. 1985; 13:3261–3271. [PubMed: 2987879]
33. Raae AJ, Kleppe RK, Kleppe K. Kinetics and Effect of Salts and Polyamines on T4 Polynucleotide Ligase. Eur. J. Biochem. 1975; 60:437–443. [PubMed: 173544]
34. Cherepanov AV, de Vries S. Kinetics and Thermodynamics of Nick Sealing by T4 DNA Ligase. Eur. J. Biochem. 2003; 270:4315–4325. [PubMed: 14622296]
35. Wang Y, Xie JJ, Han Z, Liu JH, Liu XP. Expression, Purification and Biochemical Characterization of Methanocaldococcus Jannaschii DNA Ligase. Protein. Expr. Purif. 2013; 87:79–86. [PubMed: 23147204]
36. Williamson A, Rothweiler U, Leiros HK. Enzyme-Adenylate Structure of a Bacterial Atp-Dependent DNA Ligase with a Minimized DNA-Binding Surface. Acta Crystallogr. D Biol. Crystallogr. 2014; 70:3043–3056. [PubMed: 25372693]
37. Coulter, WH. Means for Counting Particles Suspended in a Fluid. US#. 2,656,508. 1953.
38. Sobczak J, Duguet M. Effect of Histone H1, Poly(Ethyleneglycol) and DNA Concentration on Intermolecular and Intramolecular Ligation by T4 DNA Ligase. Eur. J. Biochem. 1988; 175:379–385. [PubMed: 2841134]
39. Minton AP. The Influence of Macromolecular Crowding and Macromolecular Confinement on Biochemical Reactions in Physiological Media. J. Biol. Chem. 2001; 276:10577–10580. [PubMed: 11279227]
40. Akabayov B, Akabayov SR, Lee SJ, Wagner G, Richardson CC. Impact of Macromolecular Crowding on DNA Replication. Nat. Commun. 2013; 4:1615–1624. [PubMed: 23511479]
41. Schnell S, Turner TE. Reaction Kinetics in Intracellular Environments with Macromolecular Crowding: Simulations and Rate Laws. Prog. Biophys. Mol. Biol. 2004; 85:235–260. [PubMed: 15142746]
42. Bezrukov SM, Vodyanoy I, Brutyan RA, Kasianowicz JJ. Dynamics and Free Energy of Polymers Partitioning into a Nanoscale Pore. Macromolecules. 1996; 29:8517–8522.

43. Krasilnikov OV, Sabirov RZ, Ternovsky VI, Merzliak PG, Muratkhodjaev JN. A Simple Method for the Determination of the Pore Radius of Ion Channels in Planar Lipid Bilayer Membranes. FEMS Microbiol. Immunol. 1992; 5:93–100. [PubMed: 1384601]
44. Bezrukov SM, Vodyanoy I, Parsegian VA. Counting Polymers Moving through a Single Ion Channel. Nature. 1994; 370:279–281. [PubMed: 7518571]
45. Krasilnikov OV, Rodrigues CG, Bezrukov SM. Single Polymer Molecules in a Protein Nanopore in the Limit of a Strong Polymer-Pore Attraction. Phys. Rev. Lett. 2006; 97:018301–018304. [PubMed: 16907416]
46. Robertson JW, Rodrigues CG, Stanford VM, Rubinson KA, Krasilnikov OV, Kasianowicz JJ. Single-Molecule Mass Spectrometry in Solution Using a Solitary Nanopore. Proc. Natl. Acad. Sci. U.S.A. 2007; 104:8207–8211. [PubMed: 17494764]
47. Kasianowicz JJ, Brandin E, Branton D, Deamer DW. Characterization of Individual Polynucleotide Molecules Using a Membrane Channel. Proc. Natl. Acad. Sci. U.S.A. 1996; 93:13770–13773. [PubMed: 8943010]
48. Mathe J, Aksimentiev A, Nelson DR, Schulten K, Meller A. Orientation Discrimination of Single-Stranded DNA inside the Alpha-Hemolysin Membrane Channel. Proc. Natl. Acad. Sci. U.S.A. 2005; 102:12377–12382. [PubMed: 16113083]
49. Muzard J, Martinho M, Mathé J, Bockelmann U, Viasnoff V. DNA Translocation and Unzipping through a Nanopore: Some Geometrical Effects. Biophys. J. 2010; 98:2170–2178. [PubMed: 20483325]
50. An N, Fleming AM, White HS, Burrows CJ. Crown Ether-Electrolyte Interactions Permit Nanopore Detection of Individual DNA Abasic Sites in Single Molecules. Proc. Natl. Acad. Sci. U.S.A. 2012; 109:11504–11509. [PubMed: 22711805]
51. Schibel AE, Fleming AM, Jin Q, An N, Liu J, Blakemore CP, White HS, Burrows CJ. Sequence-Specific Single-Molecule Analysis of 8-Oxo-7,8-Dihydroguanine Lesions in DNA Based on Unzipping Kinetics of Complementary Probes in Ion Channel Recordings. J. Am. Chem. Soc. 2011; 133:14778–14784. [PubMed: 21875081]
52. Wang Y, Tian K, Hunter LL, Ritzo B, Gu LQ. Probing Molecular Pathways for DNA Orientational Trapping, Unzipping and Translocation in Nanopores by Using a Tunable Overhang Sensor. Nanoscale. 2014; 6:11372–11379. [PubMed: 25144935]
53. Johnson RP, Fleming AM, Burrows CJ, White HS. Effect of an Electrolyte Cation on Detecting DNA Damage with the Latch Constriction of Alpha-Hemolysin. J. Phys. Chem. Lett. 2014; 5:3781–3786. [PubMed: 25400876]
54. Zhang B, Galusha J, Shiozawa PG, Wang G, Bergren AJ, Jones RM, White RJ, Ervin EN, Cauley CC, White HS. Bench-Top Method for Fabricating Glass-Sealed Nanodisk Electrodes, Glass Nanopore Electrodes, and Glass Nanopore Membranes of Controlled Size. Anal. Chem. 2007; 79:4778–4787. [PubMed: 17550232]

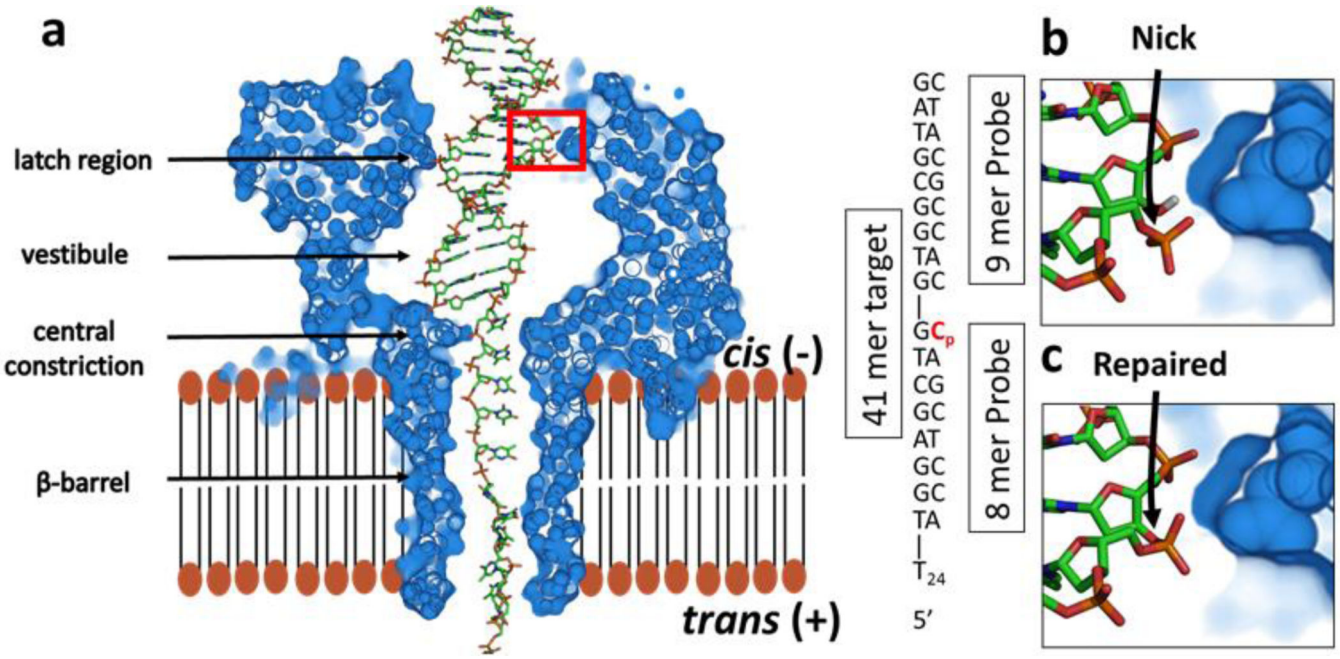

Figure 1.

(a) Outline of the α-HL channel with dsDNA captured in the vestibule. The red box shows the position of the nick within the dsDNA relative to the latch constriction. (b & c) Expanded view showing the difference in structure between duplexes with a nick at the latch region and the intact/repaired dsDNA.

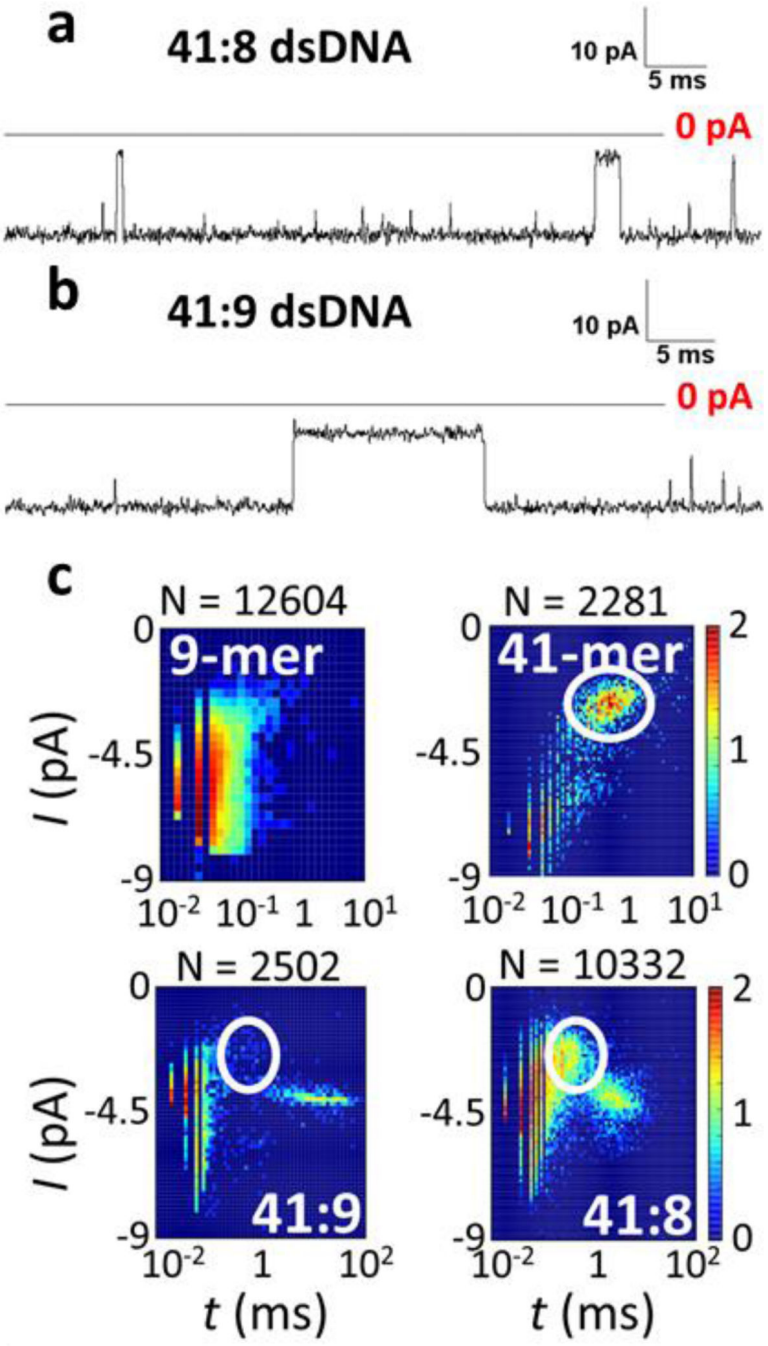

Figure 2.

Comparison between the unzipping events of 41:8 and 41:9 duplexes. (a–b) Sample current-time (*I-t*) traces generated by the 41:8 duplex (a) or the 41:9 duplex (b) in individual experiments. Events < 0.5 ms in duration are generated from ssDNA translocation and/or collision of DNA with the protein channel. The traces were post-filtered at 5 kHz for presentation. (c) Plots of event population density for *I* as a function of time (*t*) for 14 μM of 9-mer ssDNA, 41-mer ssDNA, 41:9 dsDNA and 41:8 dsDNA, respectively. Event distribution of dwelling times for 41-mer ssDNA translocation events are circled in white.

Experiments were carried out at 20.0 °C in a 100 mM KCl (7.5% PEG, 5 mM $MgCl_2$, 1 mM ATP) solution buffered to pH 7.6 with 66 mM Tris-HCl.

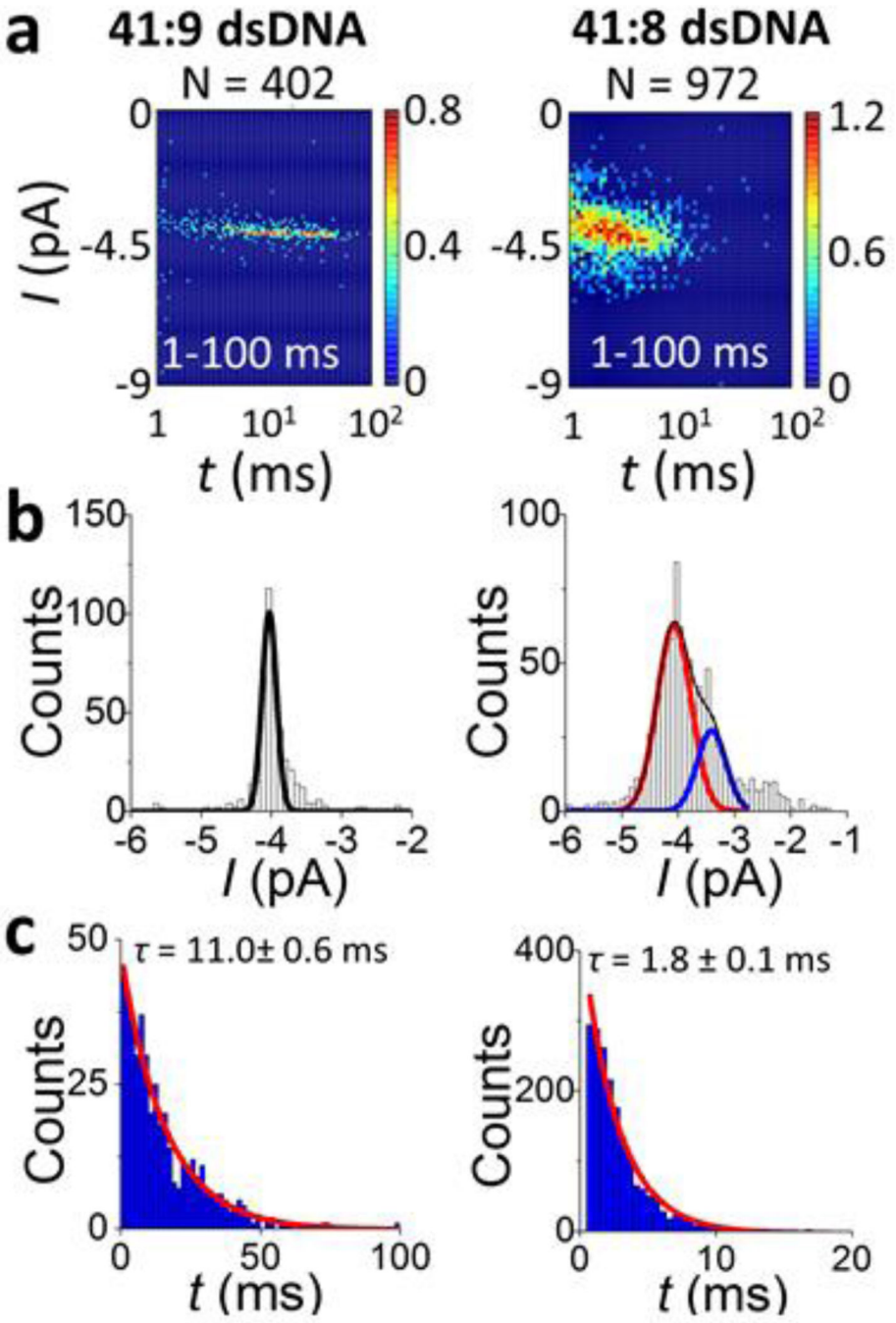

Figure 3.

Comparison between the unzipping events of 41:9 and 41:8 duplexes. (a) Plots of event population density for *I* as a function of time (*t*) and unzipping time durations for 14 μM solution of the 41:9 and 41:8 duplexes, respectively. (b–c) Current histograms and unzipping duration histograms showing the measured blockade currents for the 41:9 and 41:8 duplexes, respectively. Experiments were carried out at 20.0 °C in a 100 mM KCl (7.5% PEG, 5 mM $MgCl_2$, 1 mM ATP) solution buffered to pH 7.6 with 66 mM Tris-HCl. Counts indicate the number of individual dsDNA unzipping events.

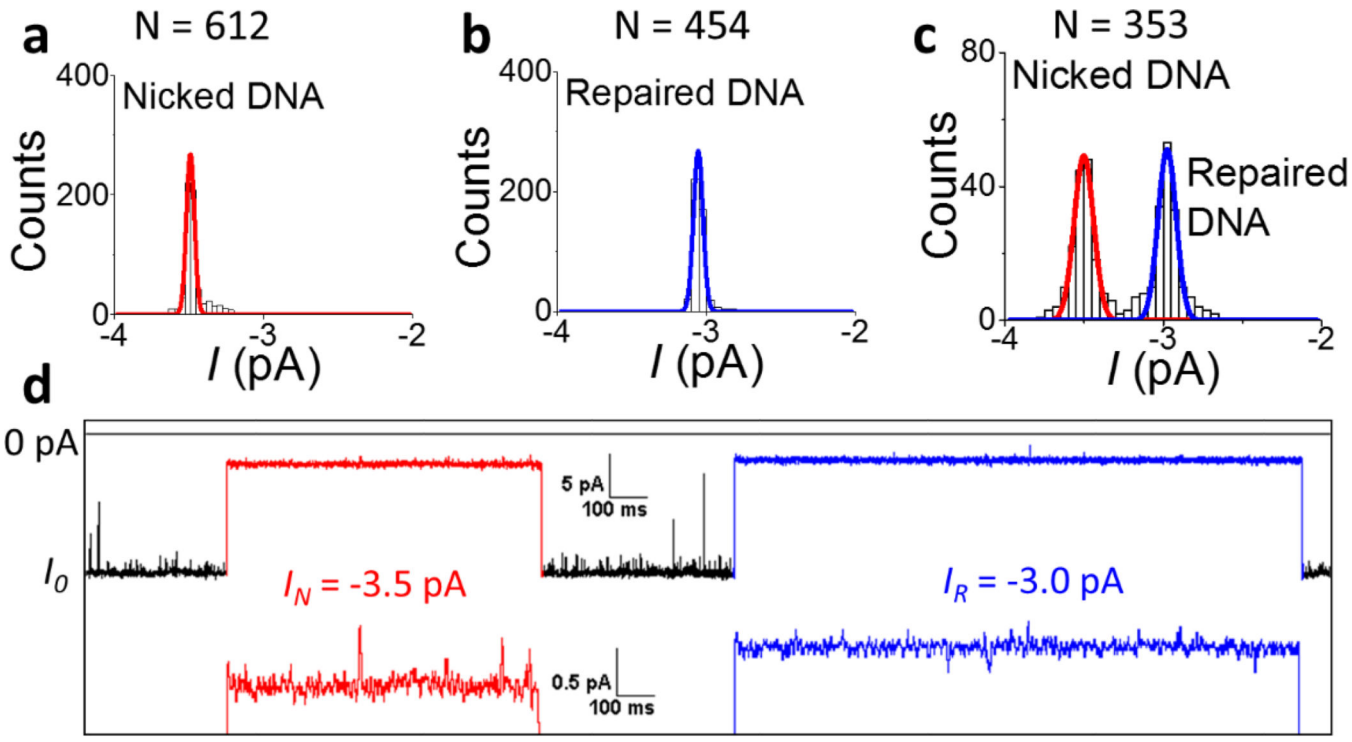

Figure 4.

Detecting backbone damage in a DNA duplex. (a–b) Current histograms showing the measured blockade currents for 14 μM solutions of the (a) nicked and (b) repaired duplexes, respectively. (c) Current histogram of a mixture of the same amount (7 μM) of nicked and repaired duplexes. (d) Sample current-time traces generated during dsDNA residence events, showing the difference in blockade currents, I_N and I_R, for nicked DNA and repaired DNA, respectively. The trace was post-filtered at 1 kHz for presentation. An expanded view of the same *I-t* trace is also shown in (d) to present the difference in blockade current of the two types of events. The expanded *I-t* trace was post-filtered at 0.1 kHz for presentation. Experiments were carried out at 20.0 °C in a 100 mM KCl (7.5% PEG, 5 mM $MgCl_2$, 1 mM ATP) solution buffered to pH 7.6 by 66 mM Tris-HCl. Counts indicate the number of individual dsDNA unzipping events.

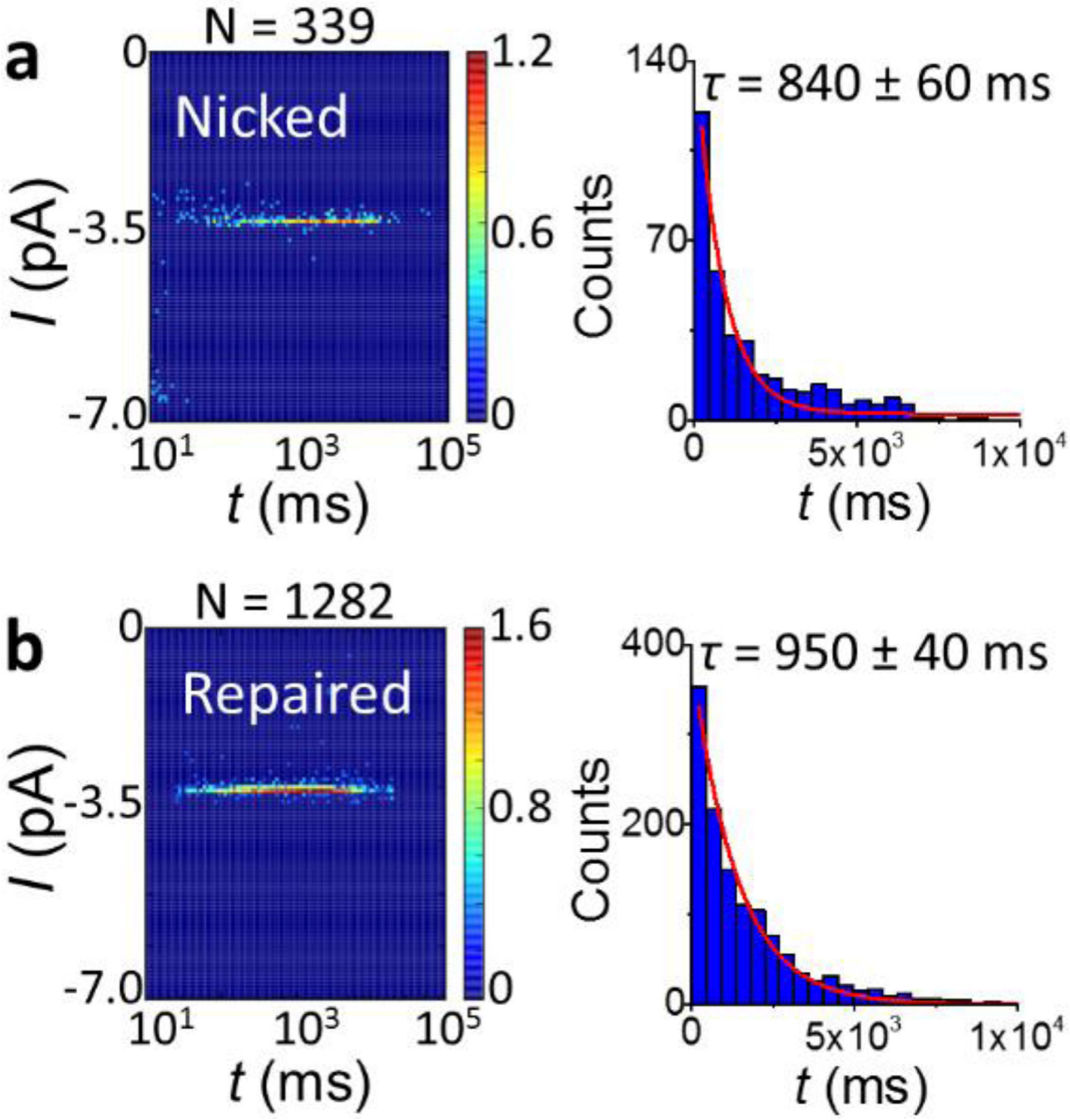

Figure 5.

Event population density plots and histograms of duration for 14 μM solutions of (a) nicked and (b) repaired duplexes. Experiments were carried out at 20.0 °C in a 100 mM KCl (7.5% PEG, 5 mM $MgCl_2$, 1 mM ATP) solution buffered to pH 7.6 by 66 mM Tris-HCl. Counts indicate the number of individual dsDNA unzipping events.

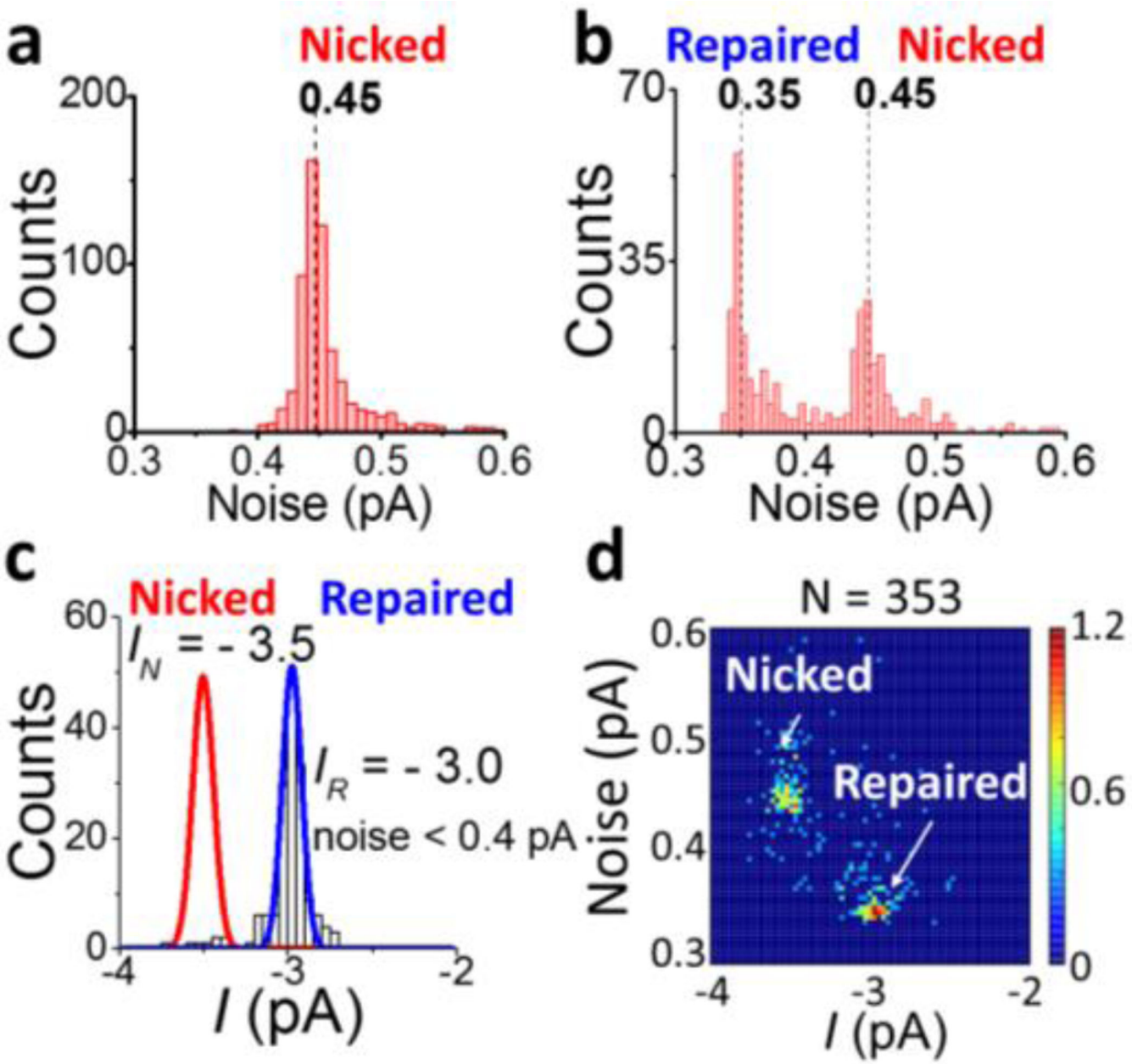

Figure 6.

Detecting backbone damage in a DNA duplex by current noise. (a–b) Histograms of current noise for duplex mixture unzipping events, containing nicked duplex alone N = 612 (a) and a mixture of nicked and repaired duplexes N = 353 (b). (c) Histogram of blockade current for the repaired duplexes in a mixture of nicked and repaired duplexes, by filtering out any current with an associated noise higher than 0.4 pA (N = 171). (d) Plots of event population density for noise as a function of blockade current for a mixture of nicked and repaired duplexes, 7 μM solution of each. Counts indicate the number of dsDNA unzipping events.

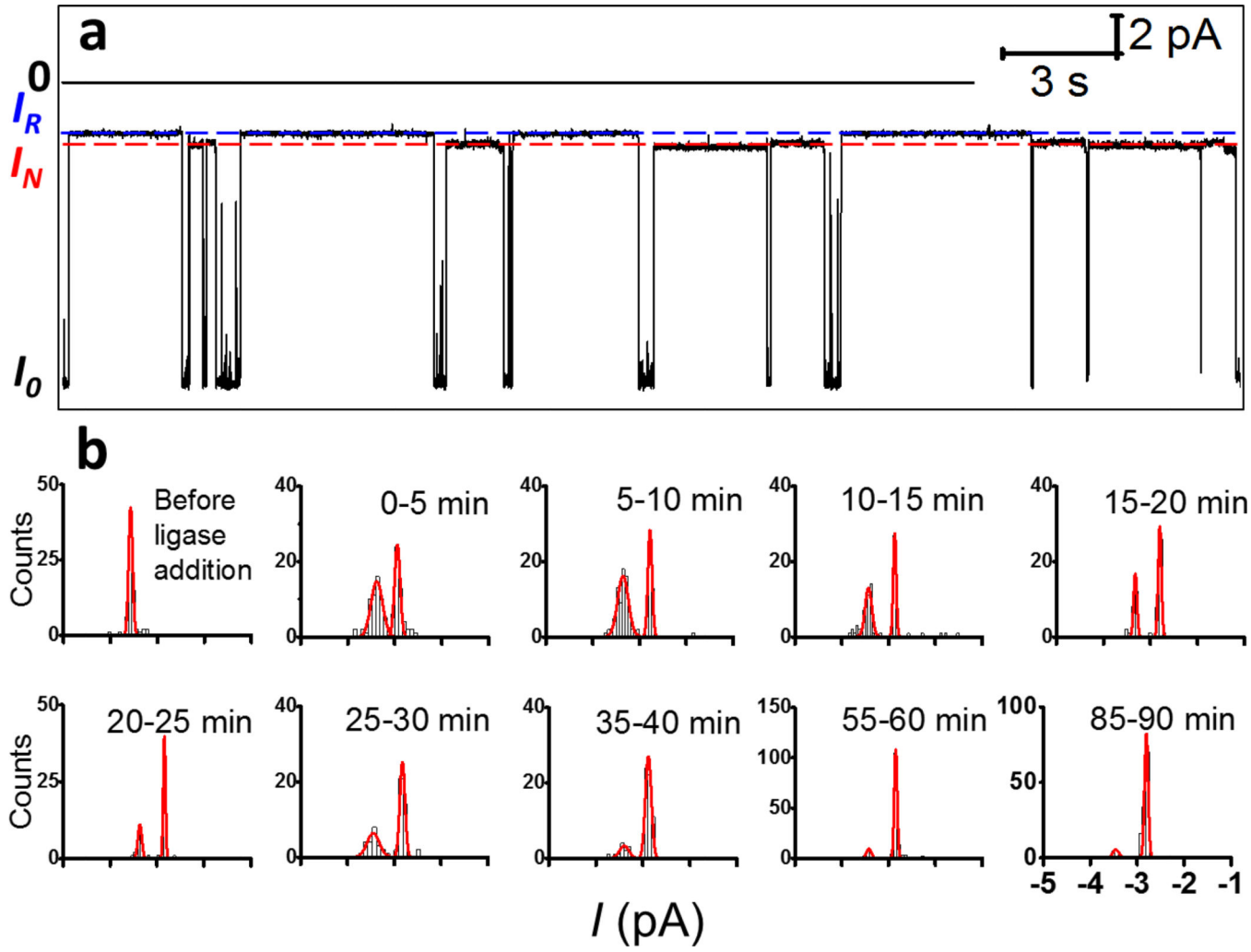

Figure 7.

Monitoring the ligase-catalyzed phosphodiester bond formation using the α-HL nanopore. In the 350-μL reaction chamber 14 μM nicked duplex was treated with 540 nM T3-DNA ligase. (a) A representative *I-t* trace during 30 s time window collected ~ 10 min after ligase addition to the *cis* reservoir. The two blockade current levels correspond to the substrate (nicked DNA, red dashed line) and product (repaired DNA, blue dashed line), respectively. Sample *I-t* trace was post-filtered at 0.1 kHz for presentation. (b) Time-dependent histograms (100–170 events) of blockade currents correspond to the progression of the enzymatic reaction. Ligase was added to the solution at $t = 0$.

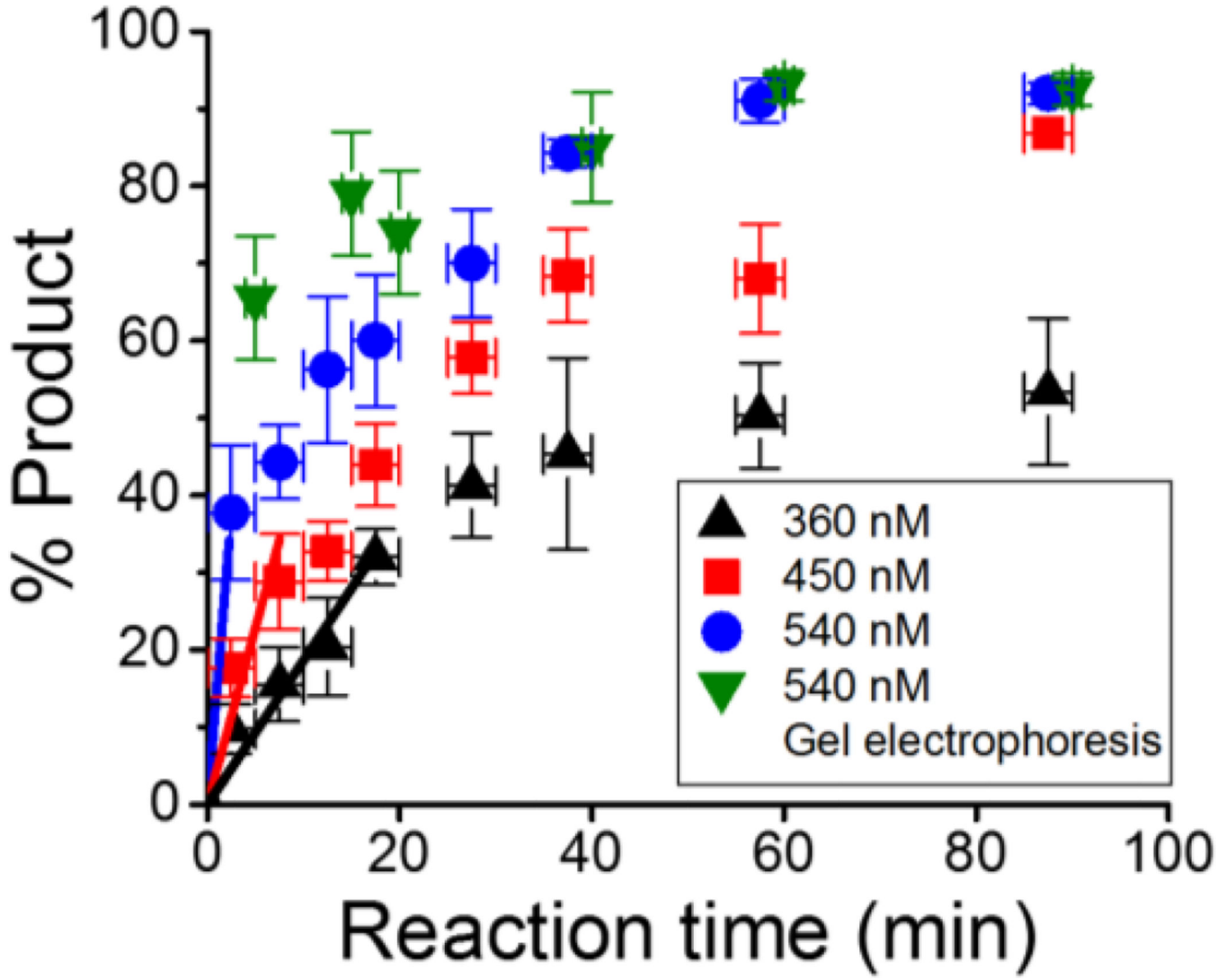

Figure 8.

Enzyme kinetic curves obtained from nanopore experiments using 14 μM nicked duplex treated with 360 (black triangle), 450 (red square), and 540 (blue circles) nM T3-DNA ligase, and the product identity is based on the blockade current separation. The *x*-axis error bars represent the 5-min time window used to generate each histogram. The *y*-axis errors were obtained from triplicate experiments (see SI Figure 8). Gel electrophoresis was conducted under the same reaction conditions with 540 nM T3-DNA ligase, and the results were plotted as green triangles. Colored straight lines correspond to a linear fit during the burst phase.